MC study of 2km muon range detector for JHF neutrino experiment

A.V.Butkevich[1]

Institute for Nuclear Research of Russian Academy of Science, 60th October Anniversary prospect,7a, Moscow 117312, Russia
and
Institute for Cosmic Ray Research, University of Tokyo, 5-1-5 Kashiwa-no-ha, Kashiwa, Chiba 277-8582, Japan

Abstract

The setup of the muon range detector (MRD) to measure the hight energy muons which are produced by neutrino beam in 2km Cherenkov detector (ChD) is presented. The algorithm for muon track and energy reconstruction is described. Contribution of the position measurement error, energy loss and multiple scattering are taken into account. The efficiency and acceptance of the muons detection by the ChD and MRD which operate in coincidence, energy and track angular resolution have been evaluated.

[1]E-mail address:butkevic@al20.inr.troitsk.ru and butkevic@iccr.u-tokyo.ac.jp

1 Introduction

After discovery neutrino oscillations by the Super-Kamiokande detector [1] and confirmation with K2K [2] new stage in neutrino oscillations studies was established. The JHF-Kamioka neutrino project is long-baseline neutrino oscillation experiment to measure parameters of neutrino oscillations with precise accuracy. Hight intensity ν_μ beam, produced by JHF 50GeV proton synchrotron, will be used. Water Cherencov detector (ChD) located at distance of 2 km from neutrino source was proposed as a near detector to measure original neutrino energy spectrum. Monte-Carlo simulations have showed that at this distance the expected neutrino spectrum is almost the same as at SK detector and 2 kilotons ChD can provide reasonable event rate.

In order to increase accuracy of determination of the incident neutrino beam at high energy the ChD can be completed with a Muon Range Detector (MDR). In this work the performance of the operation two detectors in coincidence (ChD&MRD) to measure energy and direction of muons which are produced by charge-current $\nu_\mu N$ interaction in Cherenkov detector is studied.

2 Design of the muon range detector

The 2km detectors [3] will be located in underground hole at the depth 50m. Main requirements to the near detector are as the following:

(1) detector have to be massive enough to measure the beam flux,

(2) it have to measure muon energy in the range of the expected neutrino spectra with reasonable resolution,

(3) due to limited space in underground hole length of MRD can not be more that 5m.

The schematic view of the ChD and MRD is shown in Fig.1. The Water Cherenkov detector is the cylindrical tank of 9.3m diameter and 16m length. The size of fiducial volume (FV) is 4m in diameter and 8m in length. The distance between FV and PMT surface in forward direction is 4m. The thickness of insensitive region is 1m.

The MRD consists of 22 steel plane followed by a stintillator plane. Be-

tween ChD (at the distance 74 cm from ChD) and MRD are placed two additional scintillator planes. The gap between scintillator planes and MRD is 9 cm. Fig.2 shows the schematic view of the MRD (side view). The size of the MRD is 7.5 m $\times$ 7.5 m. $\times$ 4.9 m. In order to have a good energy resolution for entire energy region, the upstream two steel plates are of 2.5 cm thick, the next two planes have thickness of 5 cm, the next ten layers are of 10 cm thick and the downstream eight are 20 cm (MRD3). The setup with the upstream four steel planes of 5 cm thick (MRD2) was regarded also. Each scintillator plane is made up of 187 strips, each one of 4 cm wide, 1cm thick, and 7.5 m long. The orientation of the strips alternates by $\pm 90^\circ$ in successive planes as shown in Fig.3. The pitch between the upstream fourteen planes is 19.1 cm and the downstream eighth is 29.1 cm. The total MRD3 (MRD2) thickness (including scintillator) of 2185 g/cm^2 (2224 g/cm^2) corresponds to muon energy of 3.5 GeV.

3 Muon tracking in MRD

The muon tracking procedure is as following. The x-z view and the y-z view are treated independently, where the z-axis is defined by the beam direction and the y-axis is defined by upward direction (see Fig.1). The least squares method described in [4],[5] is used to determine the parameters of a muon track.

The reconstructed track (x_i, y_i) is described by four parameters: the track origin (x_0, y_0) and slope of the track in xz and yz planes at its original (b_x, b_y). The points at which the track intersects each plane are parameterized as

$$x_i = x_0 + b_x(z_i - z_0), \tag{1}$$

$$y_i = y_0 + b_y(z_i - z_0), \tag{2}$$

The slope of the track are given in terms of muon direction cosines as follows

$$b_x = \left(\frac{P_x}{P_z}\right)_0, \qquad b_y = \left(\frac{P_y}{P_z}\right)_0 \tag{3}$$

The least squares estimator is linear in the track parameters

$$\chi^2 = \sum_{i,j}(x_i^m - x_i)w_{ij}(x_j^m - x_j) + \sum_{k,l}(y_k^m - y_k)w_{kl}(y_l^m - y_l), \tag{4}$$

where the weight matrix w_{ij} contains contributions from the strip width and uncertainties due to multiple scattering and energy loss, and x^m and y^m are the measured values of track position. Taking the partial derivatives with respect x_0, y_0, b_x, b_y we have the equations which can be solved analytically. We find

$$x_0 = \frac{c_1^x a_{22} - c_2^x a_{12}}{a_{11}a_{22} - a_{12}^2}, \qquad y_0 = \frac{c_1^y a_{22} - c_2^y a_{12}}{a_{11}a_{22} - a_{12}^2} \tag{5}$$

$$b_x = \frac{c_2^x a_{11} - c_1^x a_{21}}{a_{11}a_{22} - a_{12}^2}, \qquad b_y = \frac{c_2^y a_{11} - c_2^y a_{12}}{a_{11}a_{22} - a_{12}^2} \tag{6}$$

where

$$a_{11} = \sum_{i,j} 2w_{ij}, \qquad a_{22} = \sum_{i,j} 2w_{ij}z_i z_j, \tag{7}$$

$$a_{12} = a_{21} = \sum_{i,j} w_{ij}(z_i + z_j), \tag{8}$$

$$c_1^x = \sum_{i,j} 2w_{ij}(x_i + x_j), \qquad c_1^y = \sum_{i,j} 2w_{ij}(y_i + y_j), \tag{9}$$

$$c_2^x = \sum_{i,j} w_{ij}(z_i x_j + z_j x_i), \qquad c_2^y = \sum_{i,j} 2w_{ij}(z_i y_j + z_j y_i) \tag{10}$$

The muon direction cosines can be written as

$$p_z = (1 + b_x^2 + b_y^2)^{-1/2}, \qquad p_x = b_x p_z, \qquad p_y = b_y p_z \tag{11}$$

and track length can be evaluated as

$$S = (z_N - z_0)/p_z, \tag{12}$$

where z_N is z-coordinate of the last hitted scintillator plane.

The weight matrix

$$[w_{ij}] = [V_{ij}]^{-1} \tag{13}$$

where $[V_{ij}]$ is so-called covariance or error matrix. The uncertainties in the reconstruction of particle direction and track length from coordinate measurements arise due to limitations in the measurement accuracy of the detectors and errors induced by multiple scattering, i.e.

$$V = V_{er}(\epsilon) + V_{ms}(P) \tag{14}$$

Detector's uncertainties ϵ generally leave the coordinates along a real particle's trajectory uncorrelated; and they are usually described by a diagonal matrix V_{er}, with the elements $V_{ij} = \epsilon^2 \delta_{ij}$, where $\epsilon = r/\sqrt{12}$ and r=4 cm is strip's width.

Multiple scattering produces a deviation P of measured coordinates from straight track trajectory and adds correlations between measurements at different planes [4]. It is largest effect for muon in dense medium like iron. The matrix V_{mc} which takes into account the errors, induced by the multiple scattering can be written as follows

$$[V_{ms}]_{ij} = \langle P_i P_j \rangle. \tag{15}$$

Equations (71)-(73) in [5] give the variation in displacement due to multiple scattering at plane N and the covariance between the displacements at planes K and N as

$$\langle P_N^2 \rangle = \sum_{i=1}^{N} \theta_{0i}^2 \Big(\frac{x_i^2}{3} + D(i,N)(x_i + D(i,N)) \Big), \tag{16}$$

$$\langle P_N P_K \rangle = \sum_{i=1}^{K} \theta_{0i}^2 \Big(\frac{x_i^2}{3} + \frac{x_i}{2}(D(i,K) + D(i,N)) + D(i,K)D(i,N) \Big), \tag{17}$$

where x_i and $D(i,K)$ are width of steel and the distance from plane i to plane K (x_i and $D(i,k)$ are calculated along the path of muon), correspondingly. In evaluation of the mean square scattering angle at the ith plane the effect of energy loss can be accounted for as follows

$$\theta_{0i} = \frac{\theta_0}{1 - \sum_{j=1}^{i} a_{ion} x_i / p_0}, \tag{18}$$

where a_{ion} is the muon ionization energy losses, p_0 is an initial muon momentum in GeV, and

$$\theta_0 = \frac{0.0136}{p_0 \beta} \Big(\frac{x_i}{X_0} \Big)^{1/2} \Big[1 + 0.038 \ln \Big(\frac{x_i}{X_0} \Big) \Big], \tag{19}$$

with the radiation length of iron X_0=1.76 cm.

The method of the muon track and energy reconstruction is an iterative one, and proceeds as follows:

1) If number of the hitted scintillator planes $4 \leq N_h \leq 23$, the track parameters x_0, y_0, b_x, b_y and track length S are calculated using $V = V_{er}(\epsilon)$ (Eqs.(5)-(13)).

2) The muon energies $E_1 = f(S)$ and $E_2 = f(S + X_{N+1})$, where X_{N+1} is width of steel plane, in which muon has stopped, along muon path (see Fig.4a), are evaluated. The relationship between the muon energy and the muon range in MRD $f(S)$ is shown in Fig.5. The muon energy is estimated as $E_\mu = (E_1 + E_2)/2$

3) Repeat with $V = V_{er}(\epsilon) + V_{ms}(P)$. The reconstructed direction and energy E_μ is used for calculation of V_{ms} matrix.

4) Containment analyses requires a track to be contained in detector to make an energy measurement possible. The reconstructed track is extrapolated to the next stintillator plane as shown in Fig.4b. If an intercept is at the distance $d \leq 20$ cm from the edge of the plane, this event is identified with through going muon and excluded from the following analysis.

4 MC study of MRD acceptance and resolution

Charged-current neutrino events have been simulated in fiducial volume of ChD using the calculated neutrino energy spectrum at distance of 2km from neutrino production point for the off-axis beam [6]. The peak neutrino energy is tuned to the oscillation maximum of ~ 0.8 GeV and spectrum continues up to ~ 15 GeV. Three-dimensional MC codes for simulation of muon transport through the Cherenkov detector and MRD have been applied. The codes allow either to consider the average ionization energy loss calculation along tracking step, or to account for fluctuations either by explicit δ-ray production above a given energy out (in this simulation the δ-electrons energy cut of 1 MeV is used) or by a computed fluctuation function (Gaussian or approximating the Landau shape). Muon transport is performed with variable optimized steps. Multiple scattering [7] and lateral displacement are sampled also.

The numbers of muons produced by charge current quasi-elastic (QE) and inelastic (nQE) neutrino interactions in the FV of the 2km ChD and

detected by ChD and MRD are shown in the table. The numbers of 1-ring events are shown also. This type of events have been reconstructed (vertex position, muon momentum and direction), using the methods developed for 1kt detector (K2K neutrino experiment).

FV of Cherenkov Detector

	1-ring	**total**
QE	85172	116766
QE+nQE	110445	213791
QE/nQE	3.5	1.2

Cherenkov Detector + MRD

	1-ring	**total**
QE	3847	5475
QE+nQE	9014	27014
QE/nQE	0.75	0.25

Radius - z-coordinate distributions of the total number and the 1-ring QE+nQE events in the FV are shown in Fig.6 and Fig.7, respectively. Fig.8 shows the energy distribution of the 1-ring events. The spectrum of muons, which have stopped at distance ≥ 0.5 m before PMT plane in sensitive region of the ChD, and those, which reached the MRD3/MRD2, are shown also. The muon energy spectra that can be detected by the ChD and ChD&MRD2/MRD3 are presented in Fig.9.

The result of a muon energy reconstruction by the MRD3, i.e. the scattered plot of truth muon energy at the entry into MRD E_0 versus reconstructed energy E_{rec} is presented in Fig.10. The obtained relationship between E_0 and E_{rec} to be related to the discrete structure of the MRD. The muon energy range which can be measured by the MRD3 is $0.125 \div 3.5$ GeV. Figure 11 (top panel) shows the dependence of the mean value of $\langle \Delta E/E \rangle /$ (which is taken as energy resolution) on the muon energy, where $\Delta E = E_0 - E_{rec}$. The differences in the truth and reconstructed muon directions $\Delta\theta$ (angular resolution) is plotted in Fig.11(bottom panel) also. The vertical bars show the $\sigma(\Delta E/E)$ and $\sigma(\Delta\theta)$, correspondingly. The energy

resolution is of $\sim$ 1% and $\sigma(\Delta E/E)$=5%$\div$7% at $E \leq$3.5GeV; $\Delta\theta$ decreases with muon energy from $\sim$6° up to 1°

5 MC study of Cherenkov Detector&MRD acceptance and resolutions

Different types of muon events, generated in FV of the ChD are shown in Fig.12. The event types are
a) stopping muons in the active MRD region
b) stopping muons in the sensitive ChD region
c) stopping muons between the active water region and the active MRD region
d) penetrating muons through the barrel wall
e) stopping muons in the barrel side insensitive region
f) penetrating muon through the vertical wall of the ChD

The detection efficiencies of the different event types as a function of the muon energy are shown in Fig.13. The efficiency for type a+b) events has minimum of $\sim$ 52% in the energy bin 1.8$\div$2.1 GeV. The events type c) may be detected, using the scintillator plane between the active water region of the ChD and the active region of the MRD, like outer detector. The events type e), in principle, may be detected also by a barrel-side outer detector. But the energy resolution of such kind events will be worse in comparison with event types a) and b). The efficiencies for events a+b+c) and a+b+c+e) are shown in Fig.13 also. In the last case the minimal efficiency is equal of 75% in the energy bin 2.4$\div$ 2.7 GeV.

The muon energy reconstruction method for a) type events is an iterative one and proceeds as follows:
1. Muon energy losed in MRD E_{MRD} is determined.
2. Muon direction at the production is evaluated, using the reconstructed vertex position and the coordinates of the hitted strips on stintillator planes between the ChD and MRD active region.
3. Track length L_{ChD} in the ChD is calculated.
4. Energy losses in water dE/dX is fitted and muon energy at the production is estimated as $E_i = E_{MRD} + (dE/dX)L_{ChD}$.

5. Energy losses is fitted at energy $E_f = \sqrt{E_i E_{MRD}}$ and the muon energy E_{i+1} is evaluated.
6. Repeat until $\mid E_{i+1} - E_i \mid / E_{i+1} \leq 0.01$
The scattered plot of (E_{rec}, E_0), is shown in Fig.14, where E_{rec} is the reconstructed muon energy and E_0 is the generated one. The differences in the reconstructed and generated muon energies and directions are plotted in Fig.15 and 16, respectively. The $\langle \Delta E/E \rangle$ and $\Delta\theta$ as functions of the muon energy is given on Fig.17, where the vertical bars show the $\sigma(\Delta E/E)$ and $\sigma(\Delta\theta)$. The energy resolution of the ChD&MRD $\sigma(\Delta E/E)$ equals to $5\% - 6\%$ and don't depend on muon energy in region $1.2 \div 6$ GeV. The angular resolution $\Delta\theta$ decreases with energy from $\sim 3^\circ$ up-to $\sim 0.7^\circ$.

The detected and reconstructed energy and angular distributions of the events type a) are given in Fig.18. The comparison shows that muon spectrum detected by the ChD&MRD can be reconstructed rather well.

6 Conclusion

In this work the main parameters and characteristics of the MRD have been evaluated. The results can be summarized is follows:

MRD

- Energy acceptance of MRD is in range 0.12GeV $\div$ 3.5GeV with a resolution $\sigma(\Delta E/E) = 5 \div 6\%$.
- Track angular resolution $\Delta\theta$ is about $1^\circ \div 5^\circ$ and depends on muon energy .

ChD&MRD

- Energy acceptance of the ChD&MRD is $1.2 \div 6.0$GeV with reconstruction efficiency of 1-ring events $\varepsilon \geq 0.5$. The efficiency will be $\varepsilon \geq 0.75$ if the outer detector is used for detection of the stopping muons in the insensitive ChD region.

- Energy resolution $\sigma(\Delta E/E)$=5÷6% .

- Track angular resolution $\Delta\theta$=0.7°÷3°

7 Acknowledgments

At first I am thankful to Prof. T.Kajita, Prof. K.Kaneyuki and Dr. K.Okumura for useful discussions, their hearty hospitality and support during my stay in the RCCN of the Institute for Cosmic Ray Research. I would like to thank ICCR Neutrino Center staff and students, Dr. A.Okada, Dr. M.Honda, Dr. C.Saji, Dr. S.Nakayama, Y.Fukuda, M.Shinohara, M.Ishitsuka, and Y.Takenaga for their help and support.

References

[1] K.S. Hirata et al., Phys. Lett. **B205** (1988) 416

[2] The K2K collaboration, M.H. Ahn et al, Phys. Rev. Lett. **90** (2003) 041801.

[3] Y. Itow et al. The JHF-Kamioka neutrino project,hep-ex/0106019

[4] Review of Track Fitting Methods in Counter Experiments, CERN Yellow Report 81-06 (1981)

[5] J.Thomas, A.Para, and D.Tovee: The Principle of Muon Tracking in MINOS, NuMi-L-301, http://www-numi.fnal.gov/cgi-bin/notePublicPrint

[6] K.Okumura (private communication)

[7] A.V. Butkevich et al.,Nucl. Instrum. Meth. **A488** (2002) 282

Figure Caption

Fig.1 Sketch of the layout of the 2km Water Cherenkov detector and MRD

Fig.2 Side view of the MRD. The overall width and height are each 7.5 m, the length is 4.9 m. The steel plates are 2.5, 5, 10, and 20 cm thick. The pitches are 19.1 and 29.1 cm.

Fig.3 Sketch of the scintillator planes and plastic strip.

Fig.4 Estimation of energy of stopped muons in the MRD (a) and containment cut (b).

Fig.5 Muon range in the MRD vs. muon energy.

Fig.6 Radius - z-coordinate distribution of QE+nQE events in the fiducial volume of the Cherenkov detector

Fig.7 The same as Fig.6, but for QE+nQE 1-ring events.

Fig.8 Energy distribution of QE+nQE 1-ring muon events in the fiducial volume of the Cherenkov detector. Spectra of stopping muons (in the ChD) and muons reached the MRD2/MRD3 are shown also.

Fig.9 Energy distribution of QE+nQE 1-ring muon events in the fiducial volume of the Cherenkov detector. The green and red lines are muon spectra which can be detected by the ChD and the ChD&MRD2/MRD3. The contribution of QE 1-ring events is shown also.

Fig.10 Muon energy at the entry into the MRD3 vs. reconstructed energy.

Fig.11 Energy (top panel) and angular (bottom panel) resolutions of the MRD2(3) vs. muon energy. The vertical bars show the $\sigma(\Delta E/E)$ and $\sigma(\Delta\theta)$.

Fig.12 Event types produced by neutrino in fiducial volume (see text). The vertical (size of 1.5m) and barrel (size of 1.2m) insensitive regions of the ChD are shown also.

Fig.13 ChD&MRD reconstruction efficiencies of the different event types as functions of the muon energy. The horizontal bars show the bin size.

Fig.14 Muon energy at the production as a function of reconstructed energy.

Fig.15 Expected energy resolution of the ChD&MRD3 at the different muon energies

Fig.16 Expected angular resolution of the ChD&MRD at the different muon energies.

Fig.17 Energy (upper) and angular (lower) resolutions of the ChD&MRD2(3) vs. muon energy. The vertical bars show the $\sigma(\Delta E/E)$ and $\sigma(\Delta\theta)$.

Fig.18 Comparison of the ChD&MRD3 detected and reconstructed energy (upper) and angular (lower) muon distribution.

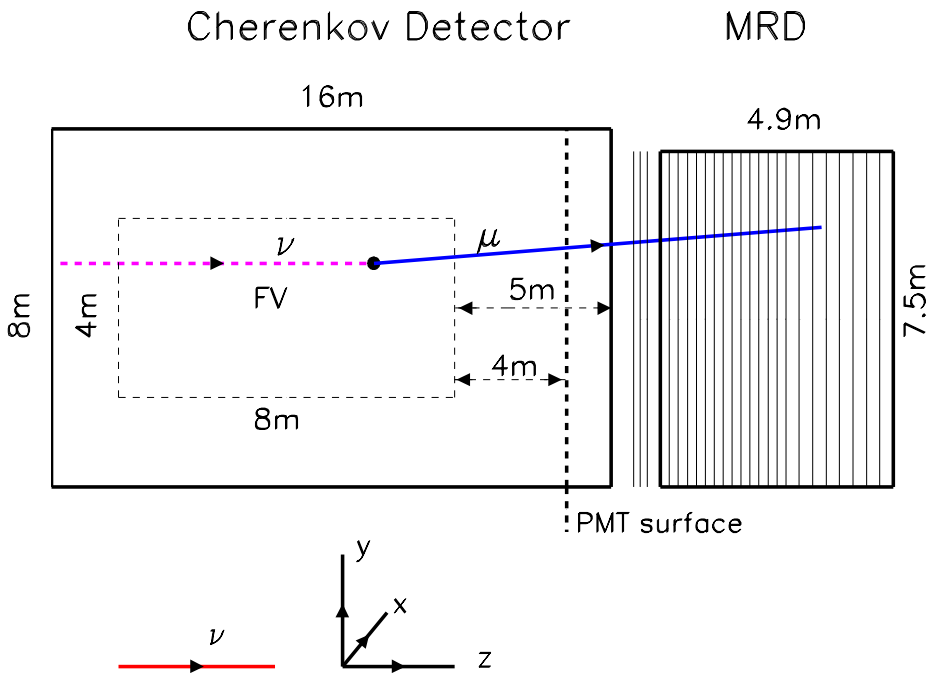
Cherenkov Detector
MRD
16m
4.9m
8m
4m
FV
5m
4m
8m
7.5m
PMT surface
y
x
z

Fig. 1

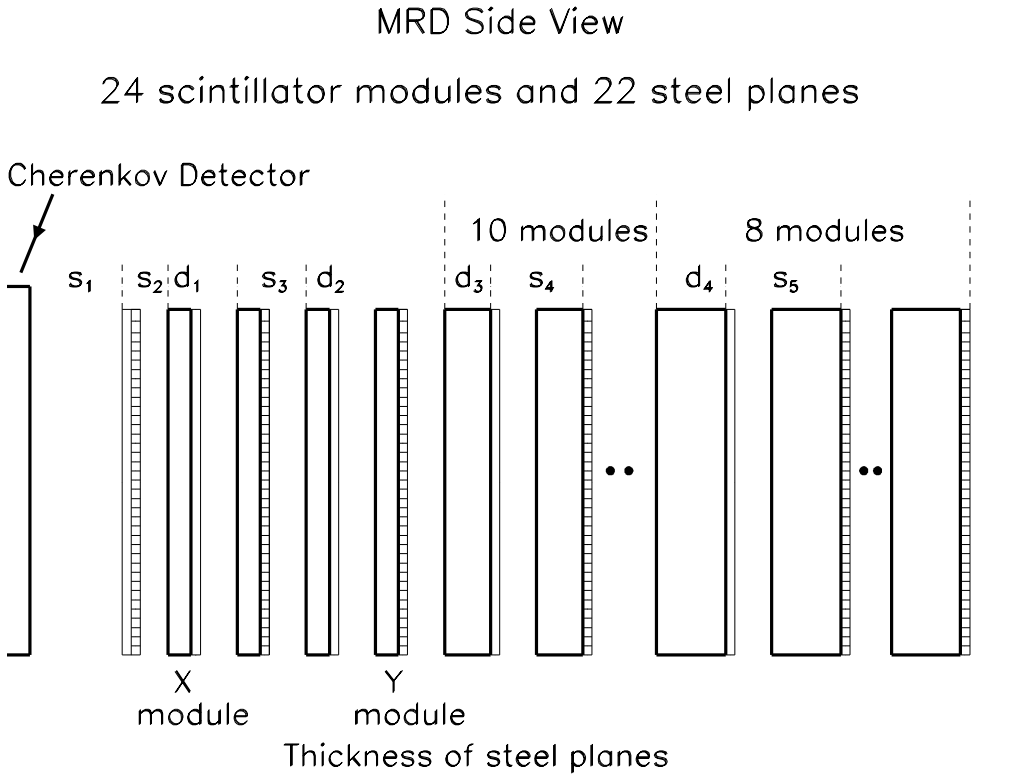
MRD Side View
24 scintillator modules and 22 steel planes
Cherenkov Detector
10 modules
8 modules
s1
s2
d1
s3
d2
d3
s4
d4
s5
X
module
Y
module
Thickness of steel planes
MRD2 d1=5cm, d2=5cm, d3=10cm, d4=20cm, H=2224g/cm2
MRD3 d1=2.5cm, d2=5cm, d3=10cm, d4=20cm, H=2185g/cm2
s1=74cm, s2=11cm, s3=19.1cm, s4=19.1cm, s5=29.1cm

Fig. 2

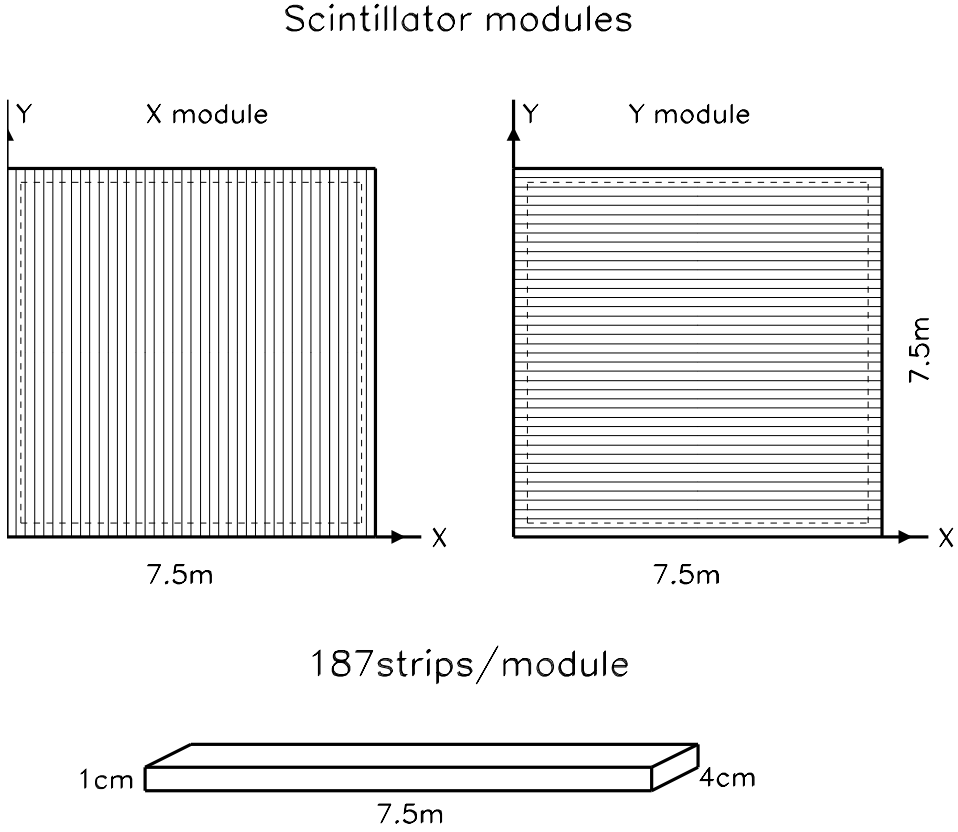
Scintillator modules
Y
X module
X
7.5m
Y
Y module
7.5m
X
7.5m
187strips/module
1cm
4cm
7.5m

Fig. 3

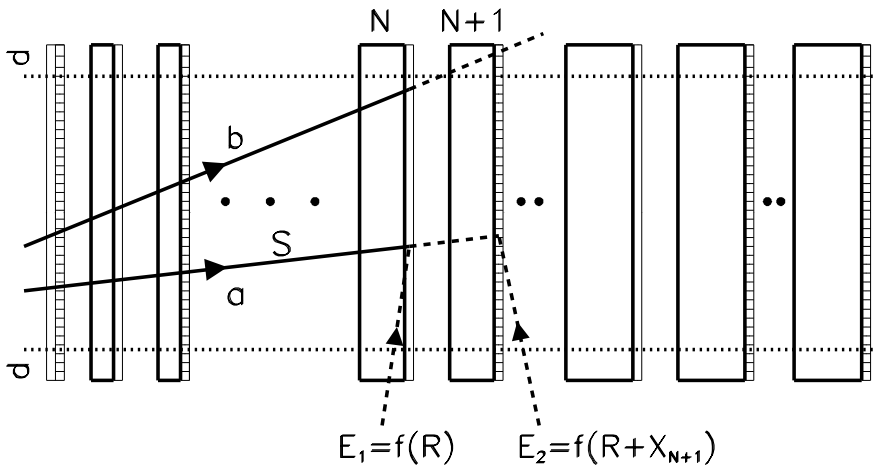

Fig. 4

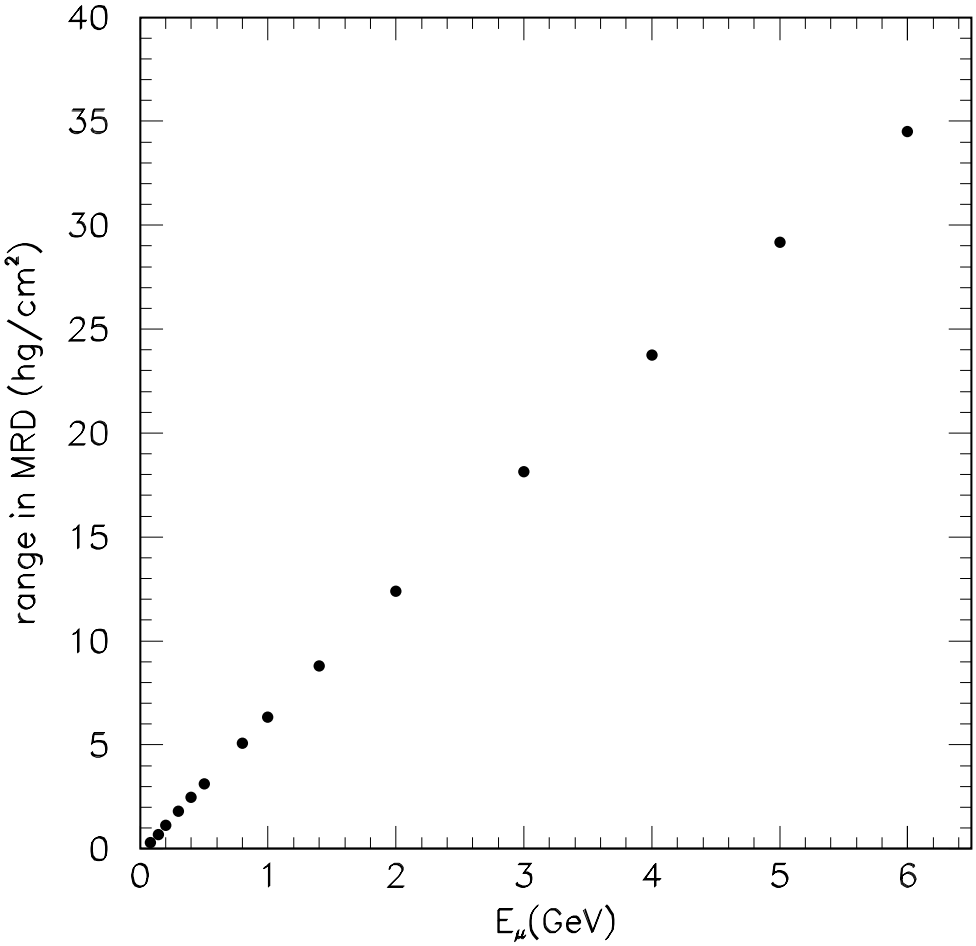

Fig. 5

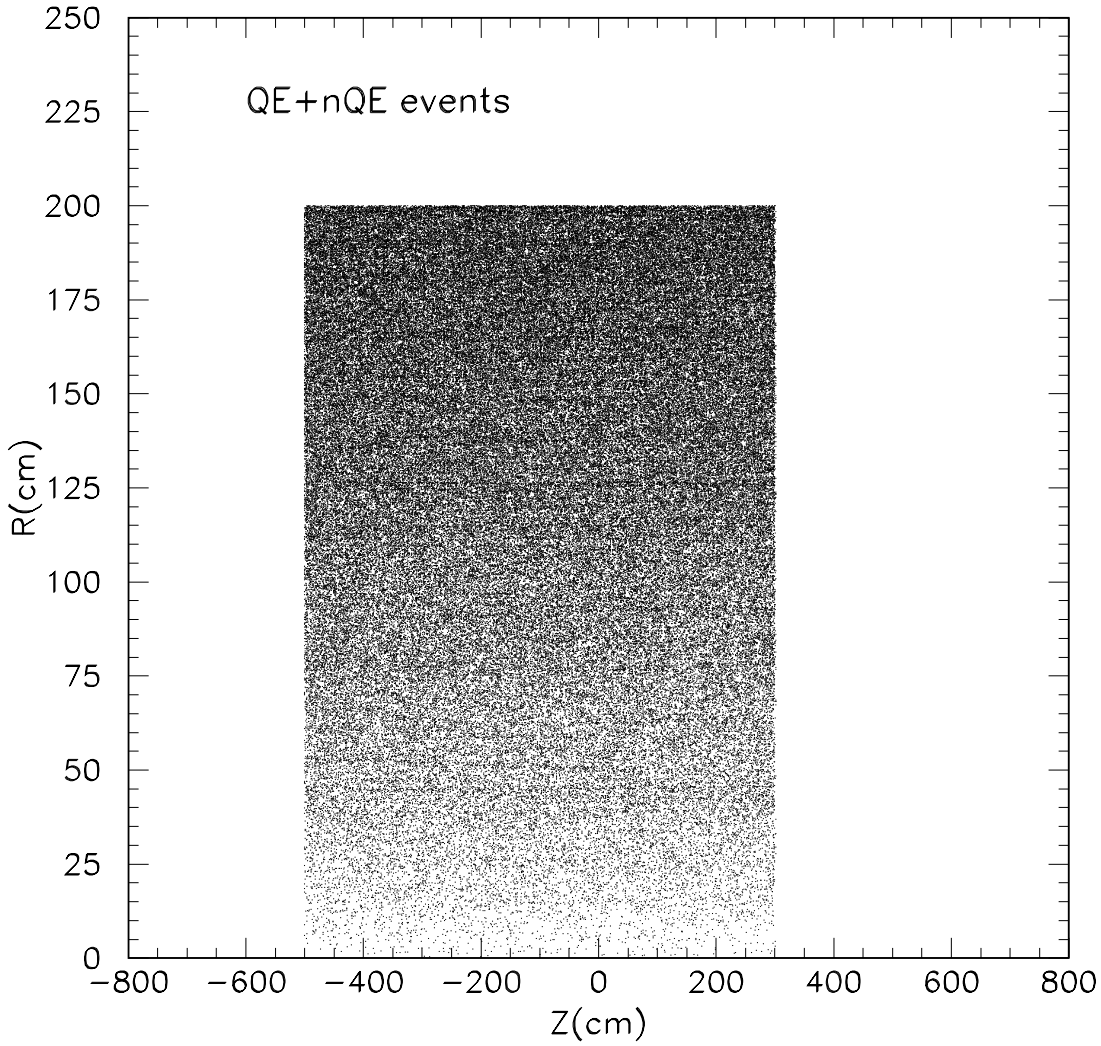
QE+nQE events
R(cm)
Z(cm)
250
225
200
175
150
125
100
75
50
25
0
−800
−600
−400
−200
0
200
400
600
800

Fig. 6

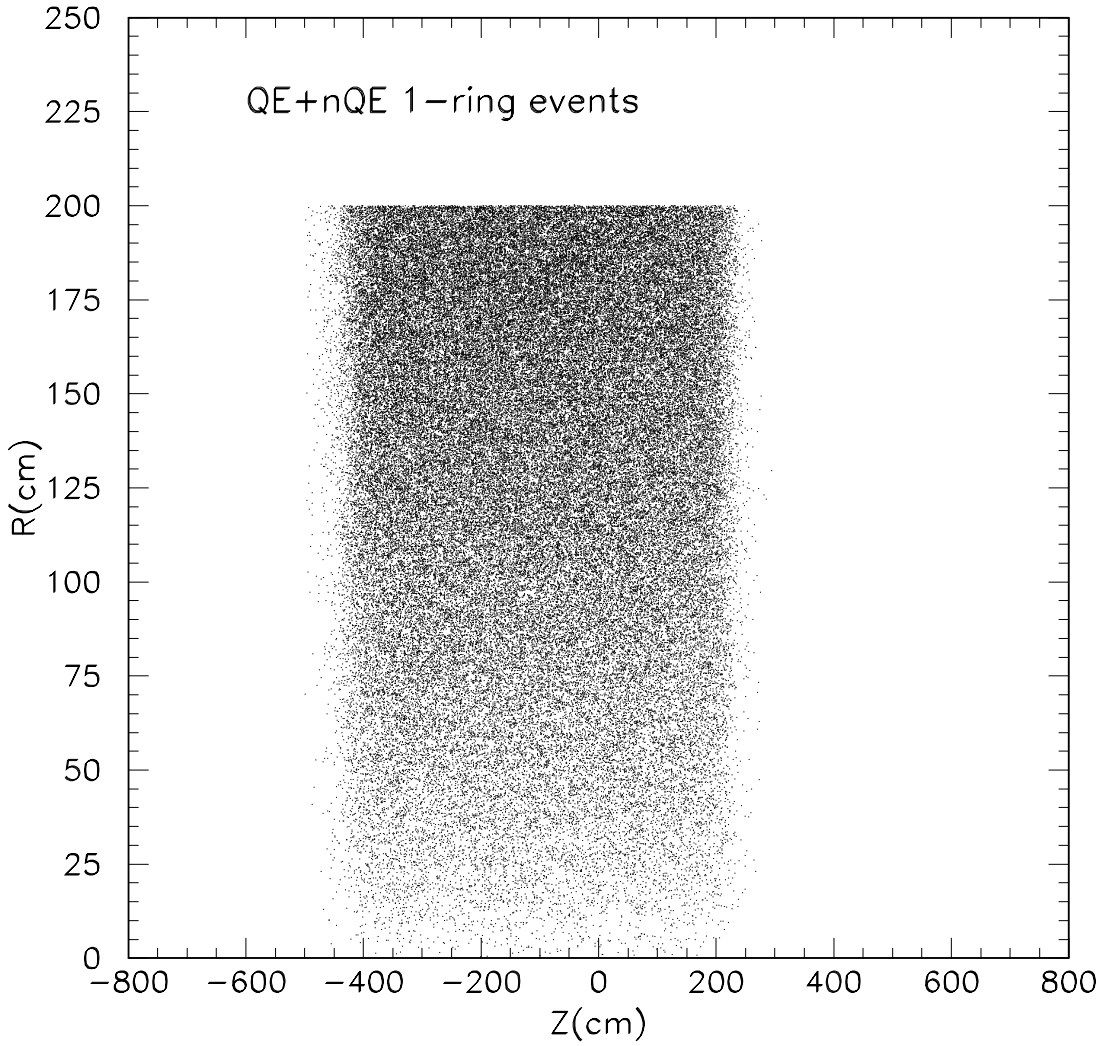
QE+nQE 1−ring events
R(cm)
Z(cm)
250
225
200
175
150
125
100
75
50
25
0
−800
−600
−400
−200
0
200
400
600
800

Fig. 7

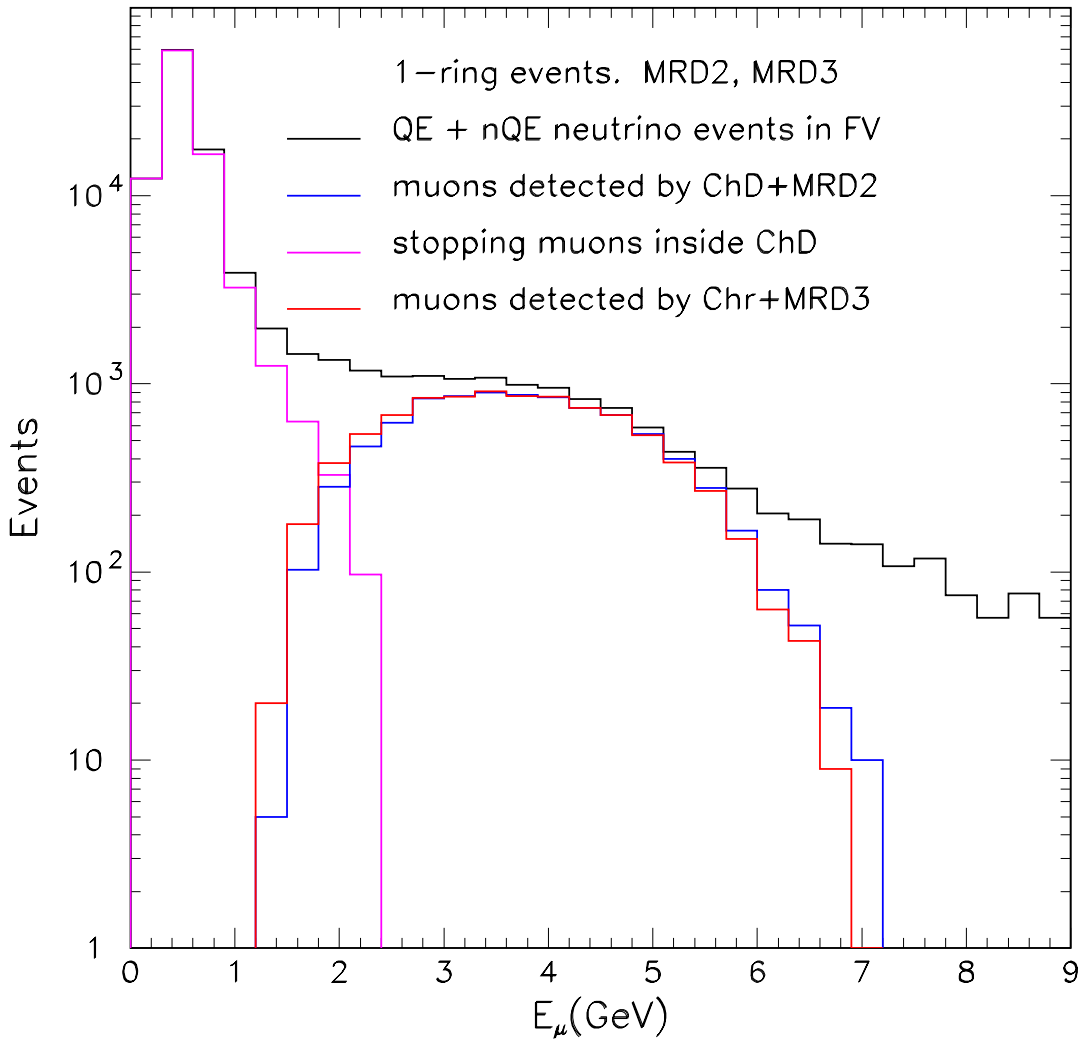
1−ring events. MRD2, MRD3
QE + nQE neutrino events in FV
muons detected by ChD+MRD2
stopping muons inside ChD
muons detected by Chr+MRD3
Events
10^4
10^3
10^2
10
1
0
1
2
3
4
5
6
7
8
9
E_μ(GeV)

Fig. 8

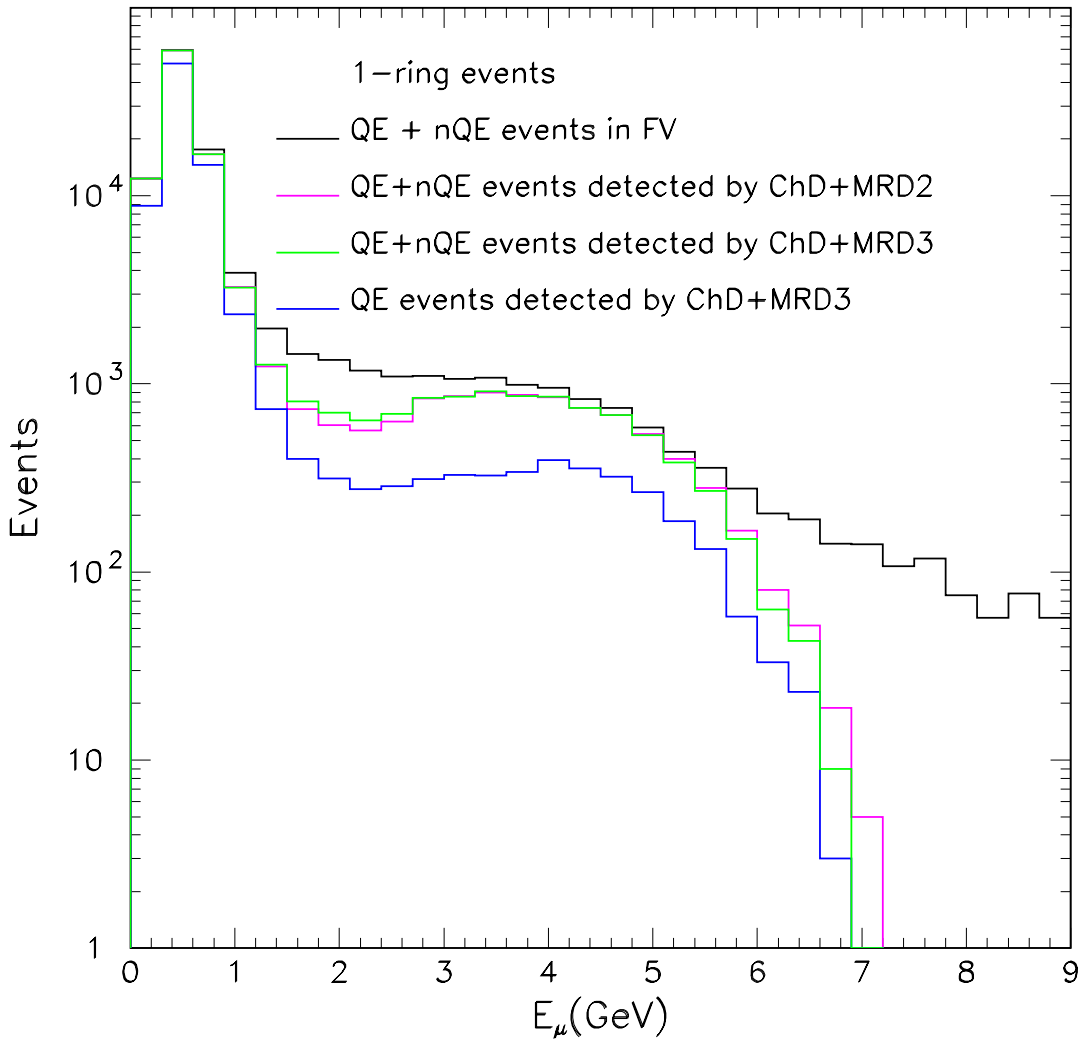
1−ring events
QE + nQE events in FV
QE+nQE events detected by ChD+MRD2
QE+nQE events detected by ChD+MRD3
QE events detected by ChD+MRD3
Events
10^4
10^3
10^2
10
1
0
1
2
3
4
5
6
7
8
9
E_μ(GeV)

Fig. 9

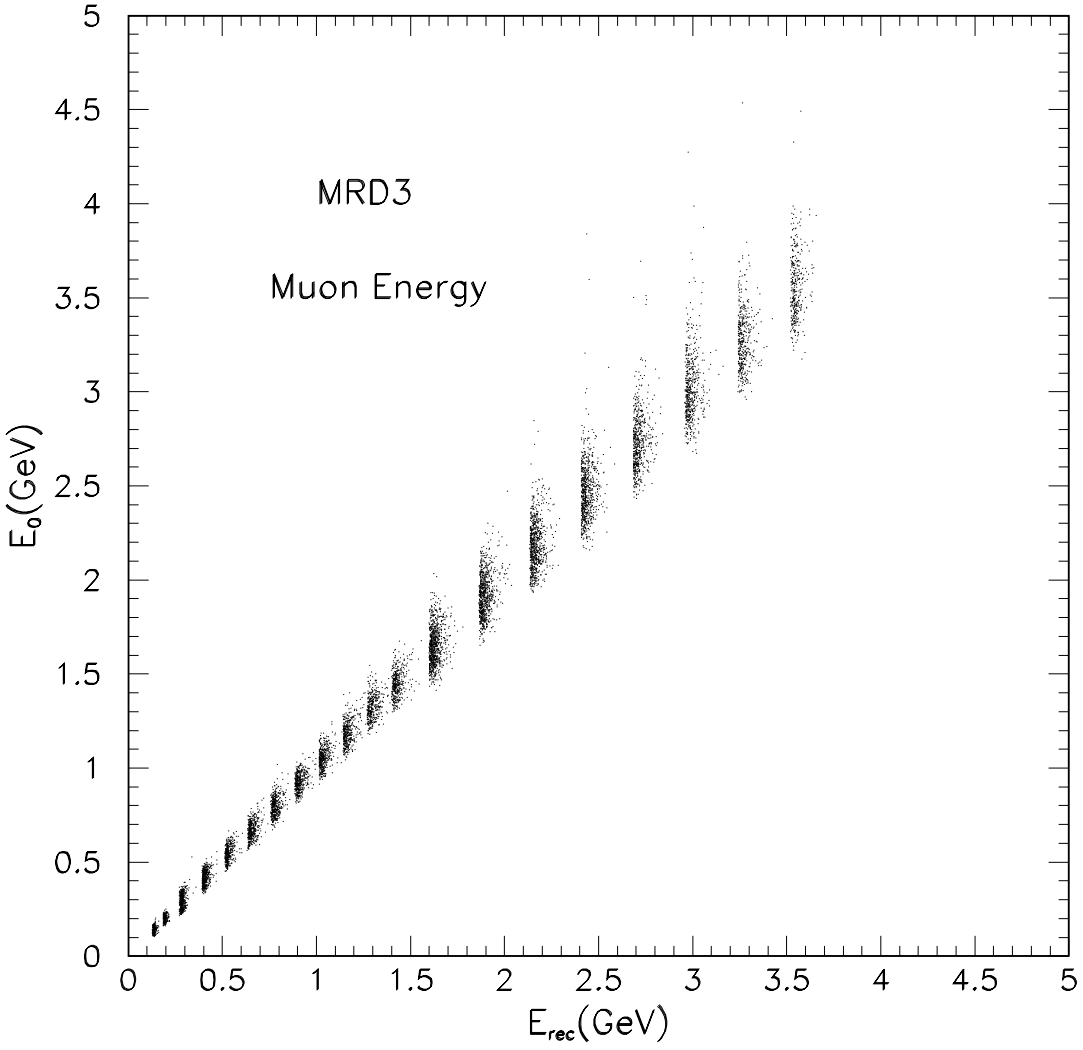

Fig. 10

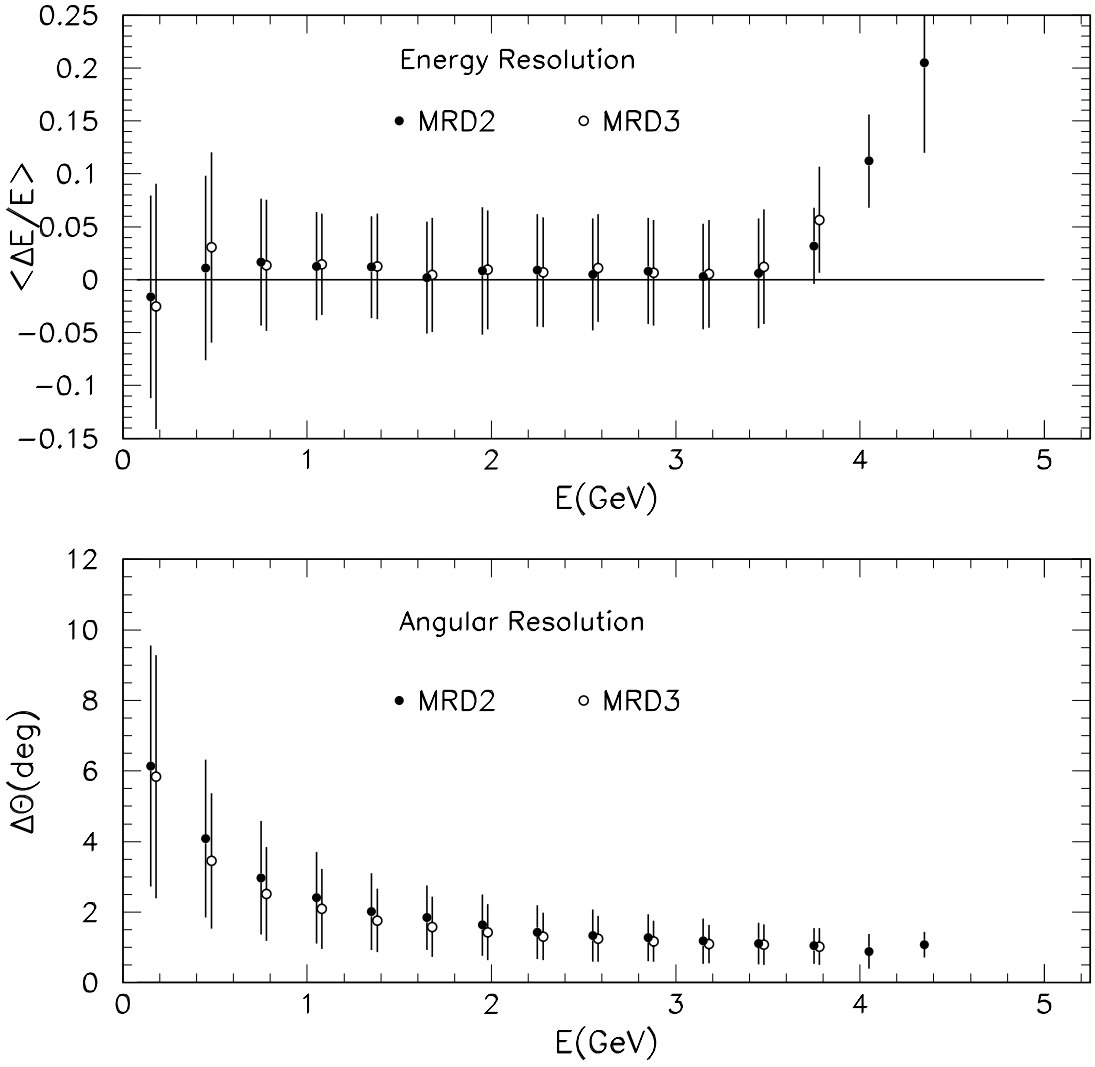
Energy Resolution
• MRD2
◦ MRD3
<ΔE/E>
E(GeV)
Angular Resolution
• MRD2
◦ MRD3
ΔΘ(deg)
E(GeV)

Fig. 11

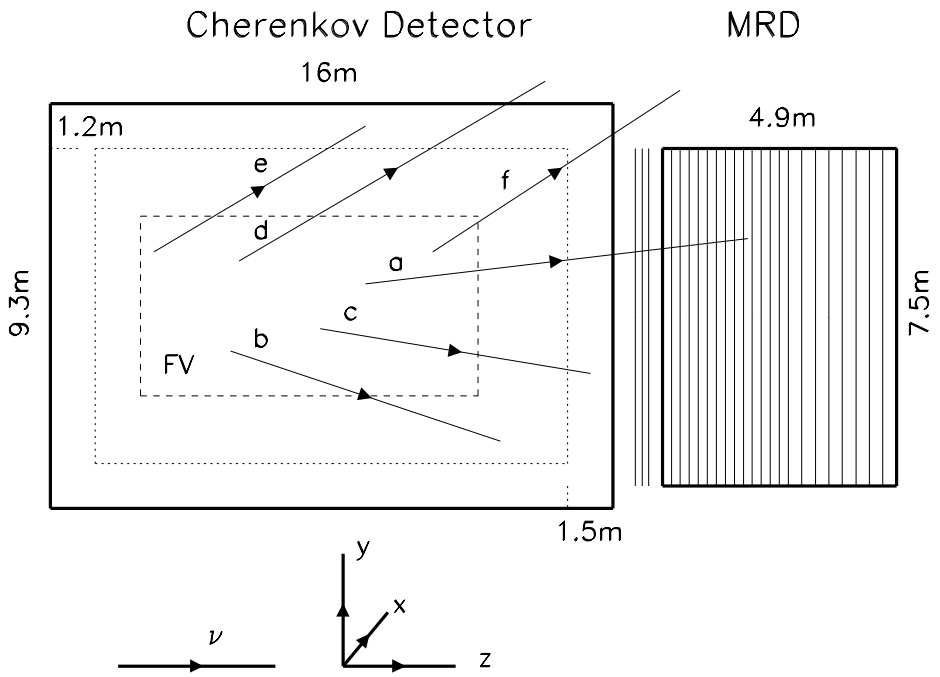
Cherenkov Detector
MRD
16m
1.2m
4.9m
e
f
d
a
c
b
FV
9.3m
7.5m
1.5m
y
x
z
ν

Fig. 12

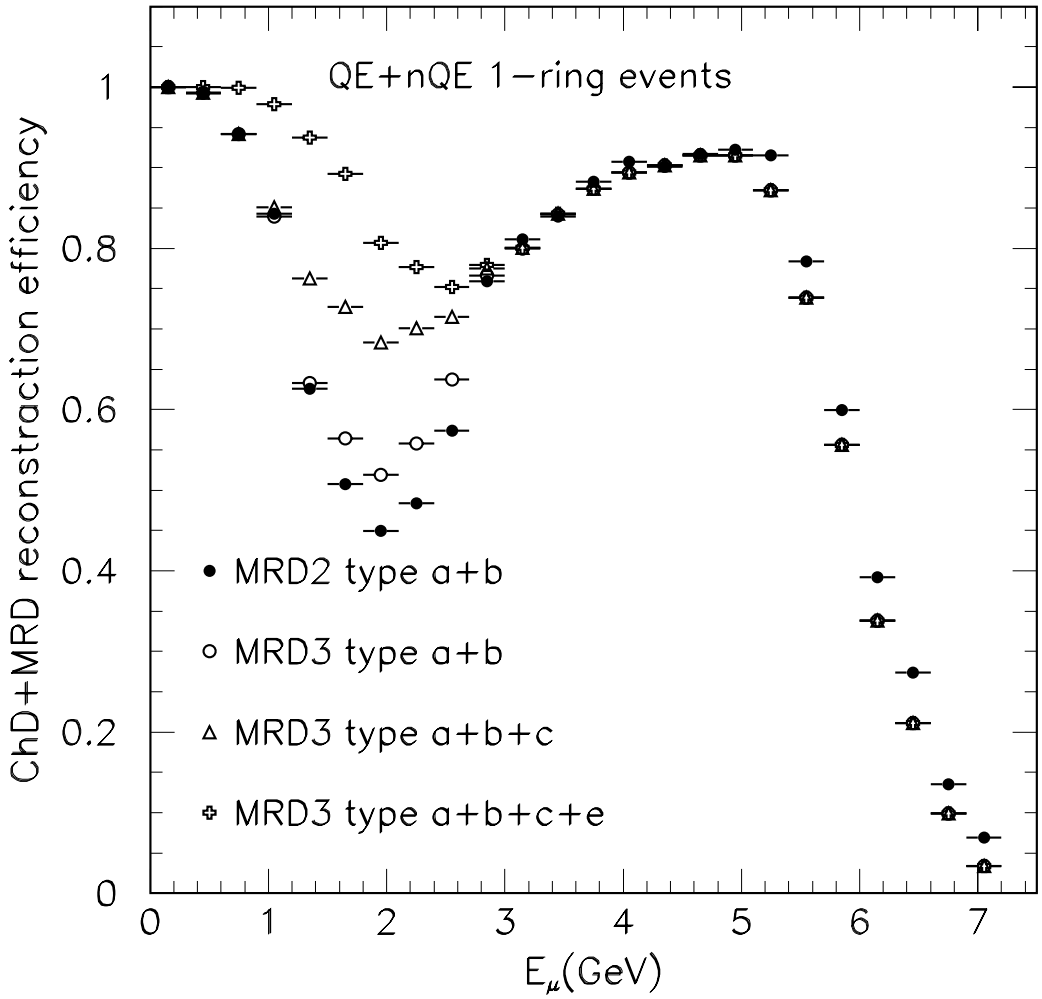
QE+nQE 1−ring events
ChD+MRD reconstraction efficiency
MRD2 type a+b
MRD3 type a+b
MRD3 type a+b+c
MRD3 type a+b+c+e
E_μ(GeV)
0
0.2
0.4
0.6
0.8
1
0
1
2
3
4
5
6
7

Fig. 13

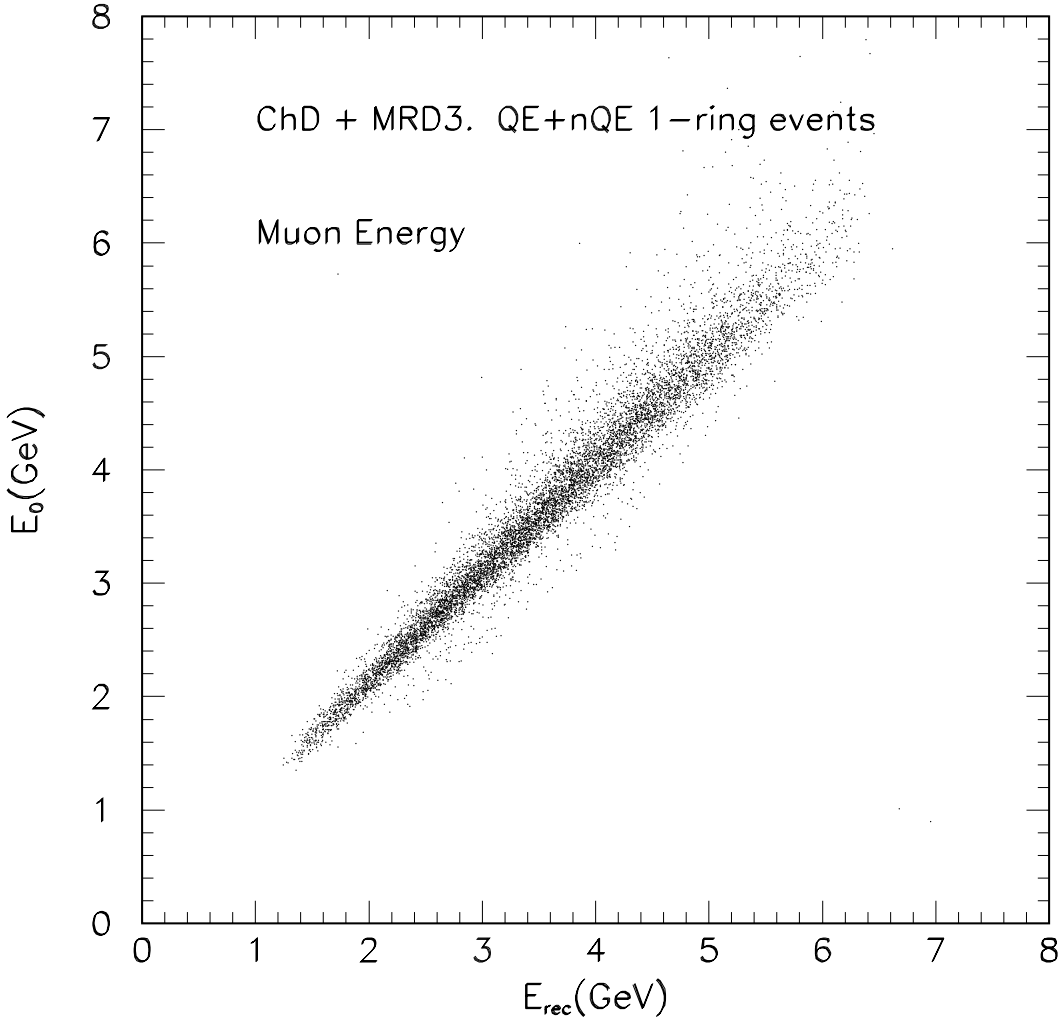
ChD + MRD3. QE+nQE 1−ring events
Muon Energy
E_0(GeV)
E_{rec}(GeV)
0
1
2
3
4
5
6
7
8

Fig. 14

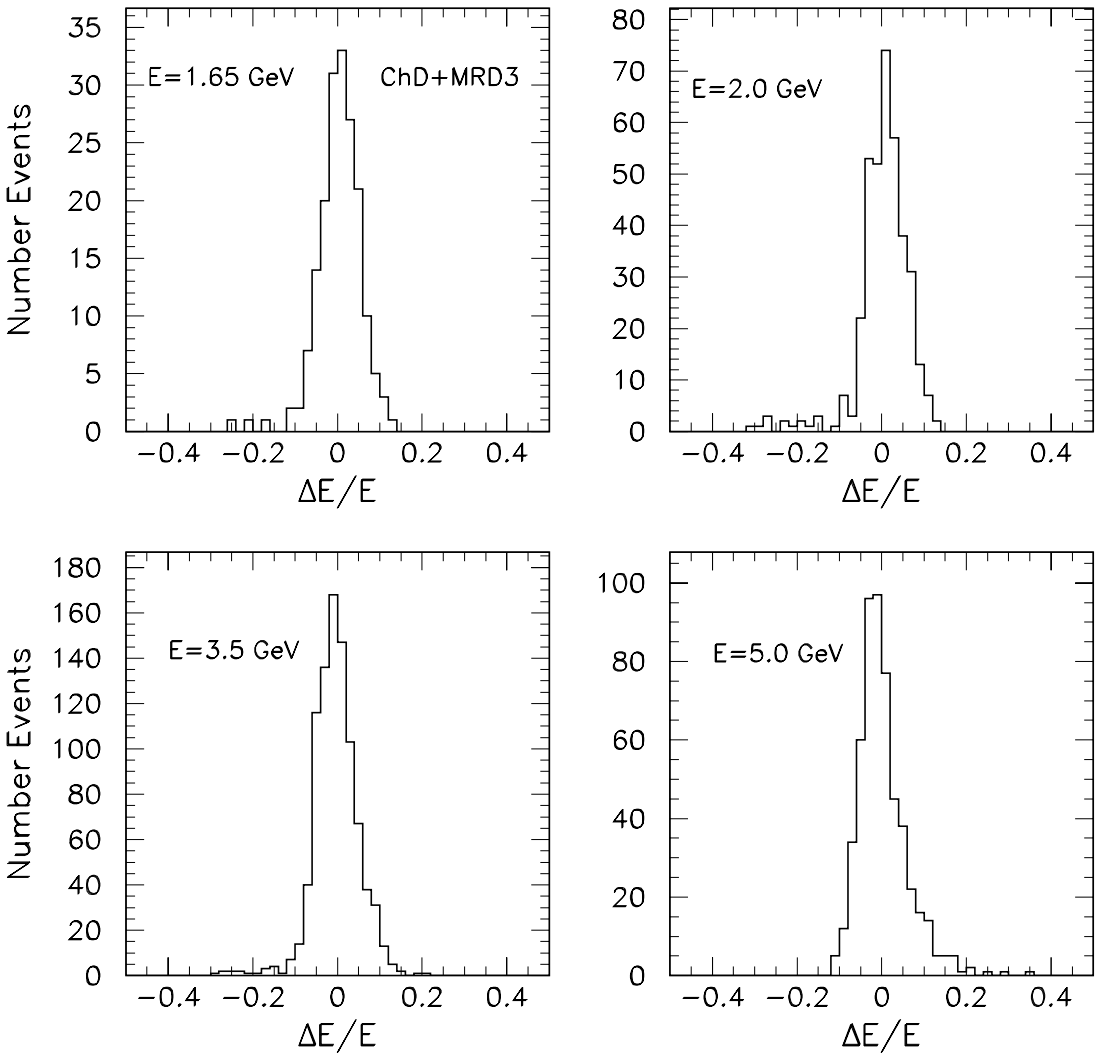

Fig. 15

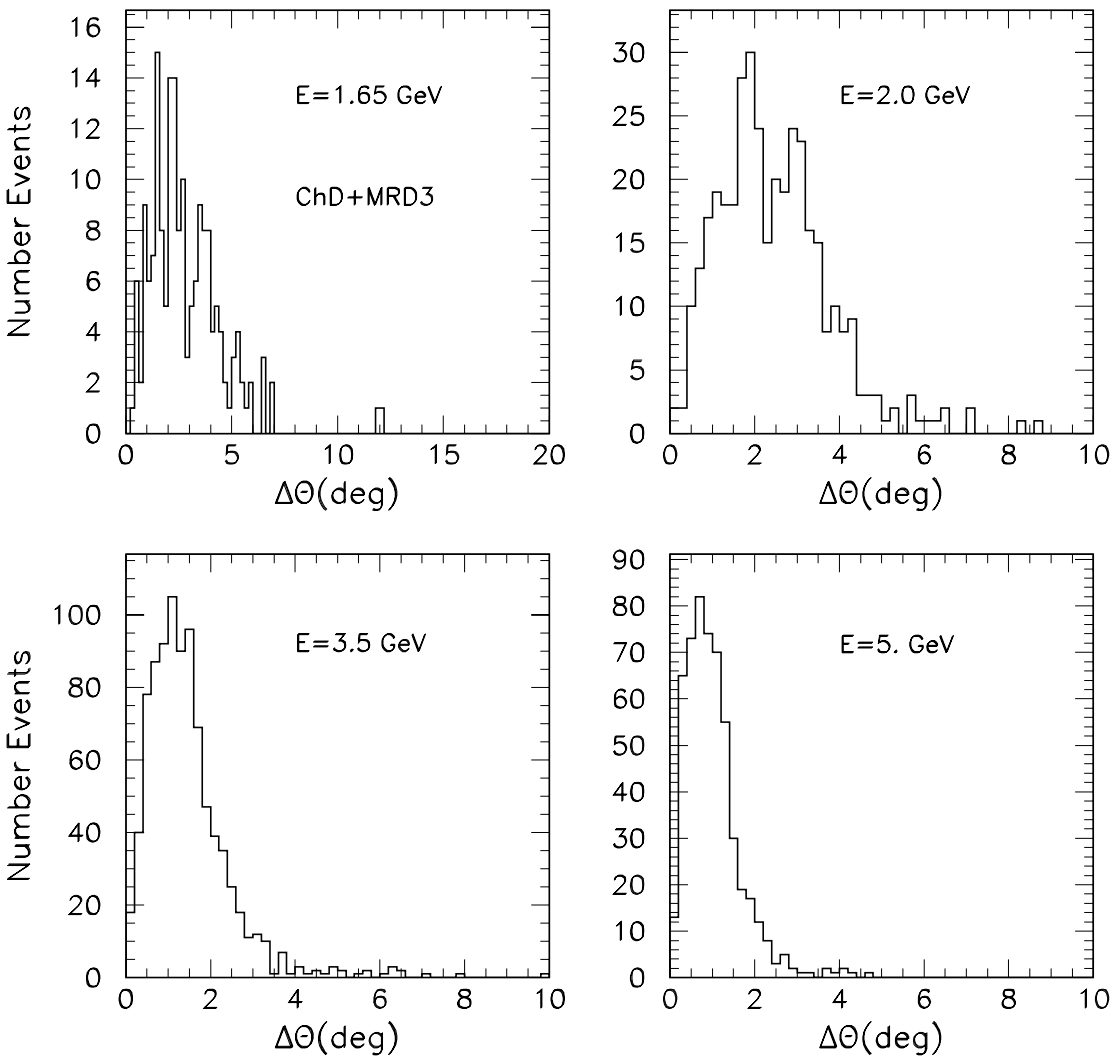

Fig. 16

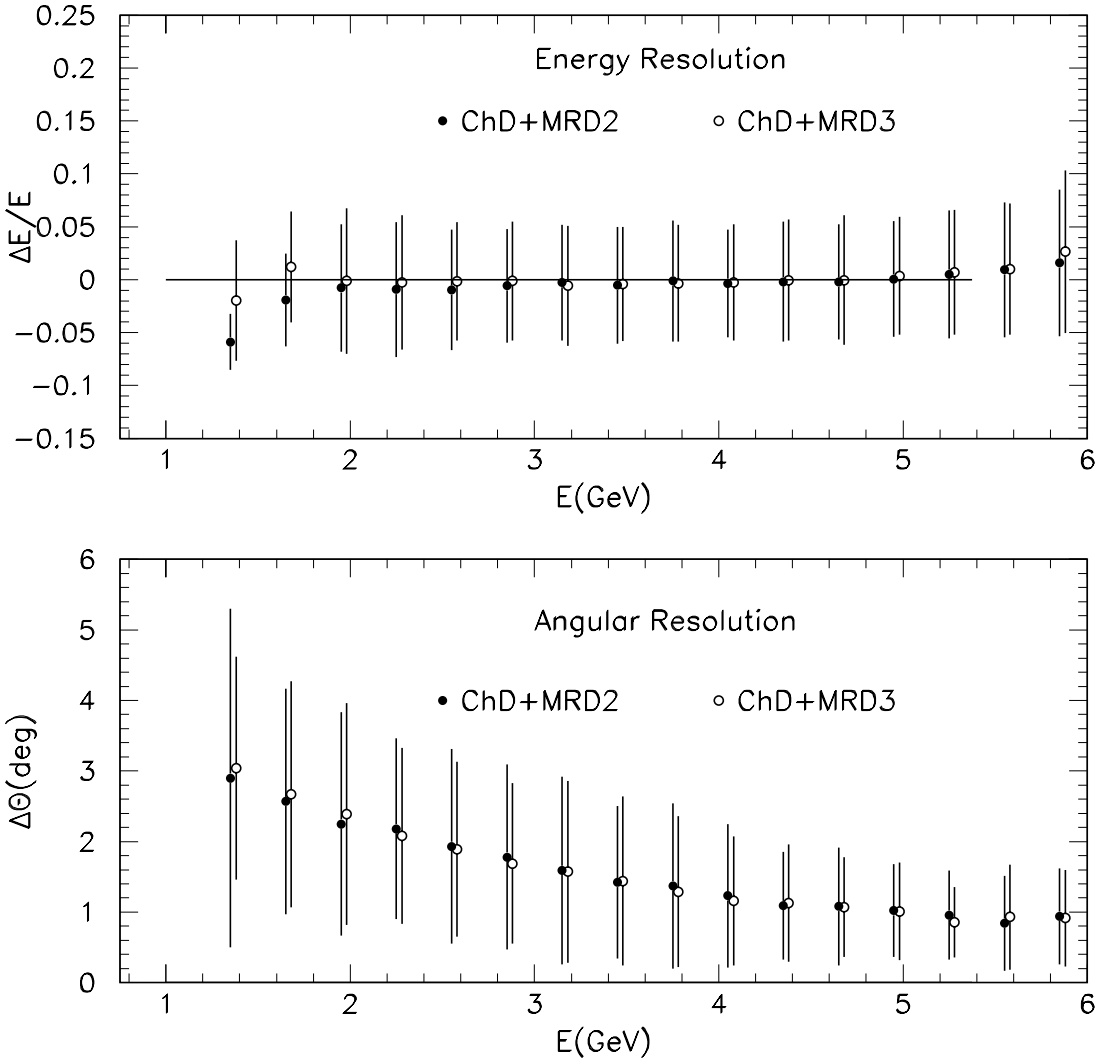
Energy Resolution
• ChD+MRD2
◦ ChD+MRD3
ΔE/E
E(GeV)
Angular Resolution
• ChD+MRD2
◦ ChD+MRD3
ΔΘ(deg)
E(GeV)

Fig. 17

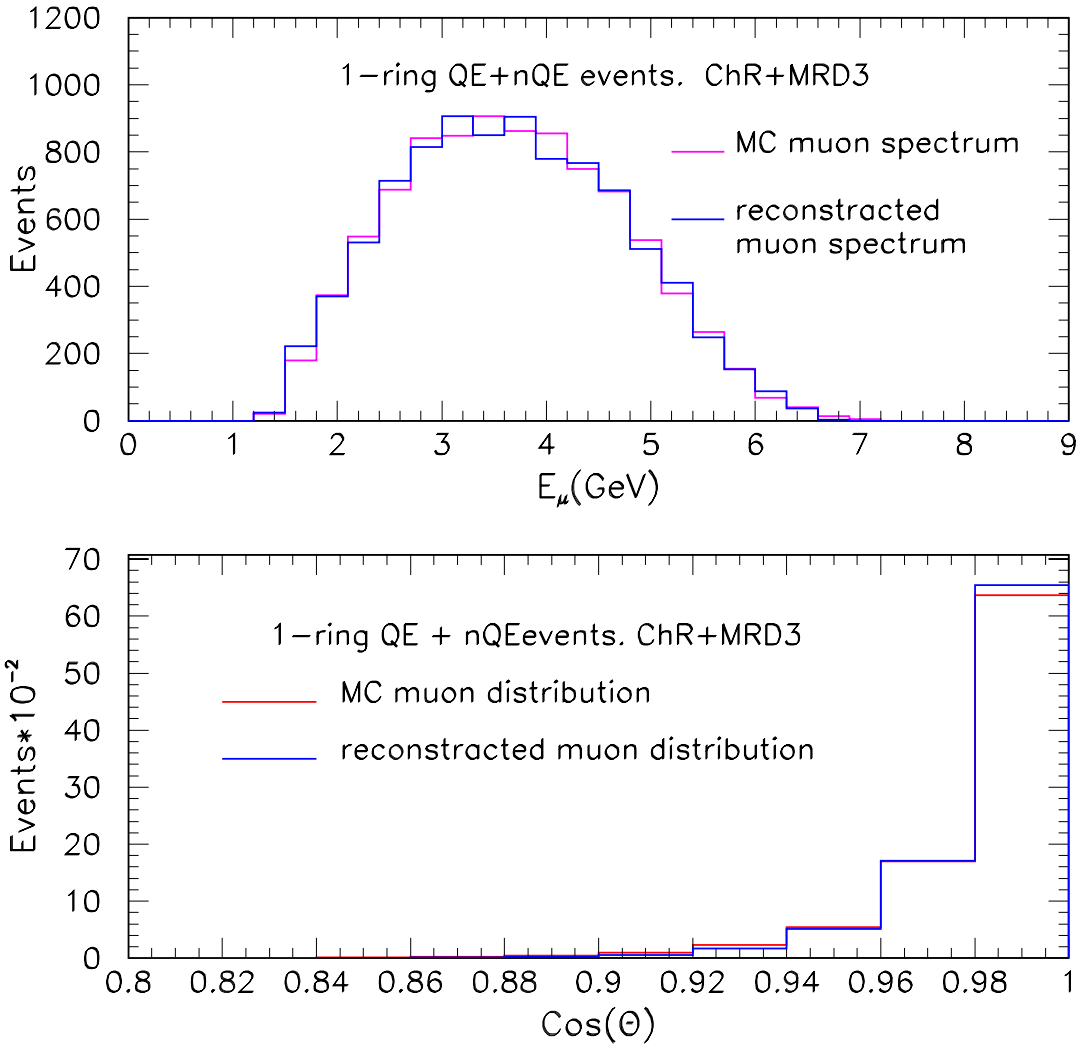
1−ring QE+nQE events. ChR+MRD3
MC muon spectrum
reconstracted
muon spectrum
Events
E_μ(GeV)
1−ring QE + nQEevents. ChR+MRD3
MC muon distribution
reconstracted muon distribution
Events*10^{-2}
Cos(Θ)

Fig. 18